Nonlinearities in GaAs cavities with high CW input powers enabled by photo-oxidation quenching through ALD encapsulation

Gregory Moille, Sylvain Combrié, Laurence Morgenroth, Gaëlle Lehoucq, Sébastien Sauvage, Moustafa El Kurdi, Philippe Boucaud, Alfredo de Rossi, Xavier Checoury

Nonlinearities in GaAs cavities with high CW input powers enabled by photo-oxidation quenching through ALD encapsulation

Gregory Moille,[1, 2, a)] Sylvain Combrié,[2] Laurence Morgenroth,[3] Gaëlle Lehoucq,[2] Sébastien Sauvage,[1] Moustafa El Kurdi,[1] Philippe Boucaud,[1] Alfredo De Rossi,[2] and Xavier Checoury[1, b)]

[1)] *Centre de Nanosciences et de Nanotechnologies, CNRS, Univ. Paris-Sud, Université Paris-Saclay, C2N - Orsay, 91405 Orsay cedex, France*

[2)] *Thales Research and Technology France, 1 avenue Augustin Fresnel, 91767 Palaiseau, France*

[3)] *Institut d'Electronique de Microélectronique et de Nanotechnologies, 59652 Villeneuve d'Ascq, France*

(Dated: 6 July 2017)

We demonstrate that encapsulation using Atomic Layer Deposition of GaAs nanocavity resonator made of photonic crystal cavity enables to prevent photo-induced oxidation. This improvement allows injecting a large quantity of energy in the resonator without any degradation of the material, thus enabling spectral stability of the resonance. Using this, we prove efficient second harmonic and third harmonic generation with a good plug efficiency ($\eta_{SHG} = 8.3 \times 10^{-5}$ W^{-1} and $\eta_{THG} = 1.2 \times 10^{-3}$ W^{-2}) and a large net output energy for both operation ($P^{out}_{SHG} = 0.2$ nW and $P^{out}_{THG} = 8$ pW).

[a)] Current address: Center for Nanoscale Science and Technology, National Institute of Standards and Technology, Gaithersburg, MD 20899, USA / Maryland Nanocenter, University of Maryland, College Park, MD 20742, USA

[b)] Electronic mail: xavier.checoury@u-psud.fr

Non-linear optics relates to large power densities, which are easily achieved in small cavities, owing to the resonant enhancement. In this context, III-V semiconductor compounds emerged to be materials of choice because of their good nonlinear figure of merit. During the past few years, the fabrication of nanoscale III-V devices has improved significantly, in particular, Photonic Crystal (PhC) Cavities. Thanks to their small modal volume[1] and the high Q-factor achievable[2–4], this type of nanoscale resonators are particularly attractive. Interestingly, frequency conversion gained in interest in the past few years. For instance, Second Harmonic Generation (SHG) is used to obtain the beating of the $f-2f$ configuration of a frequency comb[5,6] while Third Harmonic Generation (THG) for the high spatial resolution imaging[7,8]. Gallium Arsenide (GaAs) was already demonstrated to be a material of choice for resonant SHG operation in PhC cavities providing a large conversion efficiency[9]. However, for large input power, thus large optical power density, resonators made of GaAs undergo photo-induced oxidation, blue-drifting the resonance wavelength irreversibly. This oxidation process is thermally activated and follow an exponential dependence with the device temperature[10].

In this letter, we demonstrate non-linear effects in GaAs PhC cavity, namely Second Harmonic Generation (SHG) and Third Harmonic Generation (THG) with high power density at Telecom wavelengths without degrading the device. Indeed, GaAs photo-induced oxidation under large optical power density is quenched thanks to the conform encapsulation of the GaAs PhC with Atomic Layer Deposition technique where Al_2O_3 surrounds the self-suspended membrane, where the system reaches a local temperature up to about 435 K.

The device here investigated is made of a 250 nm thick GaAs self-suspended membrane grown by MetalOrganic Chemical Vapor Deposition (MOCVD). The Photonic Crystal (PhC) is patterned using electronic lithography with a period $a = 385$ nm and a hole radius $r = 0.28a$, then transferred to the PhC slab using silica hard mask and Reactive Ion Etching (RIE) process. The membrane is then released by selectively etching the sacrificial layer of GaInP below the GaAs slab. The last fabrication step consists of a conformal encapsulation with a 30 nm Al_2O_3 layer deposited by Atomic Layer Deposition (ALD). It was recently shown that such encapsulation and passivation technique helps to reduce the carrier surface recombination velocity[11]. The resonator consists of a 5 missing holes cavity, so-called L_5 cavity[12]. The two extrema holes are moved by $dx = 0.155a$ outward from the cavity (Fig. 1a) to improve the intrinsic Q factor. A modulation of the hole radii with an ampli-

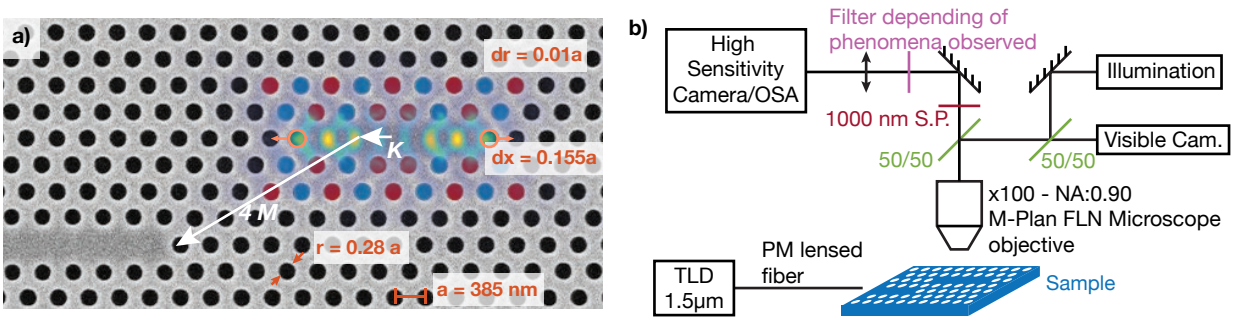

FIG. 1. a) SEM image of the L_5 PhC cavity. The extractor super-period surrounding the cavity is highlighted, in red for a positive radius variation, in blue for a negative one. The superimposed colored image corresponds to 1508 nm resonant optical spatial mode computed by FDTD – b) Experimental setup schematic. TLD: Tunable Laser Diode, PM: Polarization Maintained, SP: Short Pass filter, OSA: Optical Spectral Analyzer.

tude $dr = 0.01a$ is applied in the $\boldsymbol{M}$ directions, corresponding of twice the periodicity of the PhC. This leads to a vertical light extraction[13] at resonance. The resonator is connected to an input PhC waveguide with a width $W = 1.05a\sqrt{3}/2$ at a distance $\boldsymbol{D} = -4\boldsymbol{M} - \boldsymbol{K}$ from the center of the cavity (Fig. 1a). The end of the waveguide is composed of an inverted ~~tapers~~[14] reducing insertion losses from lensed fiber and avoiding Fabry-Perot interferences.

The cavity resonance is measured with a CW tunable laser (Santec) by detecting the di-

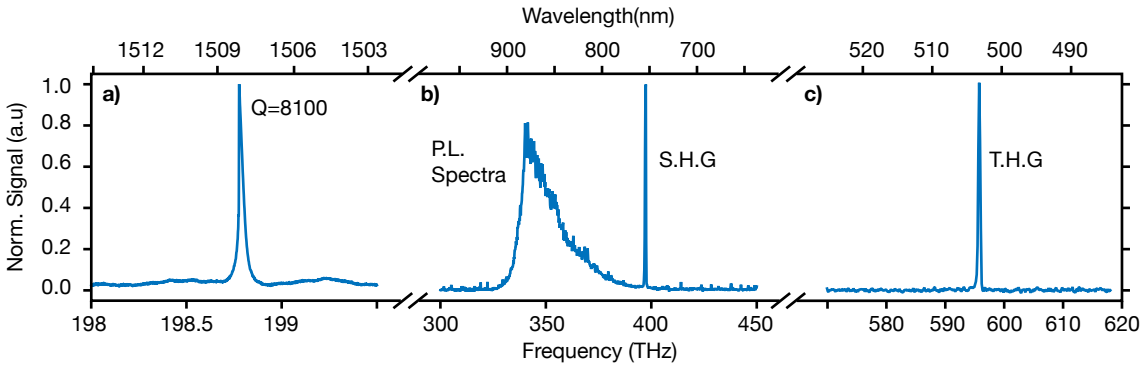

FIG. 2. Spectra of a) the cavity resonance at Telecom wavelength– b) second harmonic generation and photo-luminescence – c) third harmonic generation. a) is measured through the transmission of the device at low input power, b) and c) are measured with an optical spectrometer

rect upward transmission (Fig. 2a). We find experimentally a resonance wavelength for the second order mode at 1508.2 nm with a Q factor of $Q = 8100$. The SH (Fig. 2b) and TH

signals (Fig. 2c) are spectrally characterized using Optical Spectral Analyzers (OSA, Thorlabs, and Ocean Optics respectively), and the signal peaks lie at 754.1 nm and 502.75 nm respectively. Interestingly, the photo-luminescence (PL) can be easily detected as the excitation at 1508 nm leads to two-photon absorption, and the PL signal is spectrally separated enough from the SH one. Therefore both can be independently characterized.

Mode profiles of the SH and TH signals are observed using the setup shown in Fig. 1. The light is collected using a microscope objective (Olympus-M PLAN) with a large Numerical Aperture $NA = 0.9$ and a magnification of 100. The image is observed thanks to a high sensitivity cooled-down EMCCD camera (Andor) with a 512×512 pixels matrix. Each pixel has a size of 16 µm. The effective resolution obtained is 72 nm by pixel (*i.e.* magnification of 220). Appropriate filters are inserted in the setup to observe only the SHG (short pass filter at 1 µm) or the THG (band pass filter).

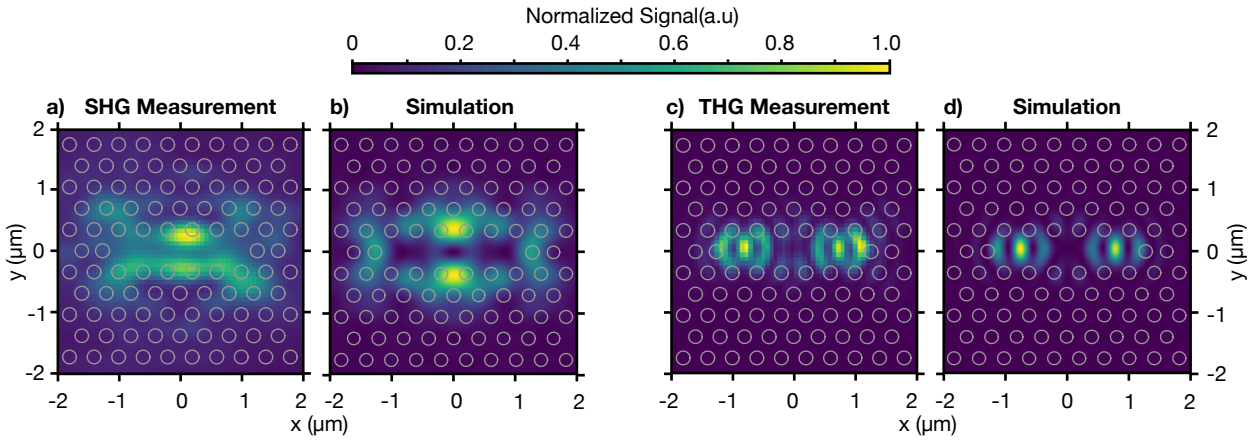

FIG. 3. a) SH mode profile measured – b) Induced polarization at SH wavelength from mode profile at the cavity resonance computed with FDTD – c) TH mode profile measured – d) Induced polarization at TH wavelength from modeling

The resulting images are shown in Fig 3a and c. SH and TH mode profile are retrieved by modeling the optical spatial mode distribution at the resonance wavelength and by computing the induced polarization[15,16] using 3D-FDTD (Fig. 3b and d). In order to compare fairly the experiment with the modeling, those last results are convoluted with the numerical aperture of the microscope objective and with the absorption length (*i.e.* 570 nm for SH signal and 110 nm for TH signal). The simulations results are in good agreement with the measurements, although for the induced polarization at the SH wavelength, the differences

between the modeling and the characterized profile are more noticeable. This could be explained by the optical index (both real and imaginary part) which could tend to differ from the value found in the literature for $\lambda = 754.1\ nm$[17,18] due to the optical pumping and two photon-absorption at 1.5 µm. It is highly interesting to note that resolving the TH spatial mode allows resolving the resonant mode at Telecom wavelength. Indeed, as previous work pointed out[8], the diffraction limit is greatly reduced using the TH signal ~~compare~~ to the Telecom one.

TABLE I. Summary of the different losses in the optical detection path for SH and TH wavelengths.

Element	**Losses (754.1 nm)**	**Losses (502.75 nm)**
Microscope obj.	-0.71 dB	-0.97 dB
50/50 mirror	-3 dB	-3 dB
1000 nm S.P. filter	-0.08 dB	-0.13 dB
End filter	-1.08 dB	-1.31 dB

The conversion efficiency of both SH and TH were characterized. Using the same setup previously shown in Fig. 1, it allows us to measure the output signal power. Indeed, the number of photons can be retrieved using the Andor camera, thus the detected power. Here, only the area corresponding to the cavity is accounted. A normalization is performed taking into account all the different losses at the SH and TH wavelength (Table I) leading to -4.87 dB for the SH and -5.41 dB for TH signal. The insertion losses to the waveguide are estimated to be -7 dB. Due to thermal effect, mostly induced by carrier recombination, the input CW signal is tuned for each input power to match the shifted resonance. The plug efficiency conversion for the SHG operation found is $P_{in}/P_{SHG}^2 = 8.3 \times 10^{-5}$ W^{-1}, while for the THG conversion is $P_{in}/P_{THG}^3 = 1.2 \times 10^{-3}$ W^{-2} (Fig. 4). Saturation effects appear at high input power, which is predicted by the Coupled Mode Theory (CMT)[19].

These efficiency values are still below the state of the art of SHG and THG for nanostructured system[9,20–22]. However, thanks to the conformal encapsulation of the system preventing photo-oxidation, high input power are achievable without any material degradation, leading to a second harmonic generation of 0.2 nW and a third harmonic generation of 8 pW, orders of magnitude higher than in ref. 9. Those output power values are in the same

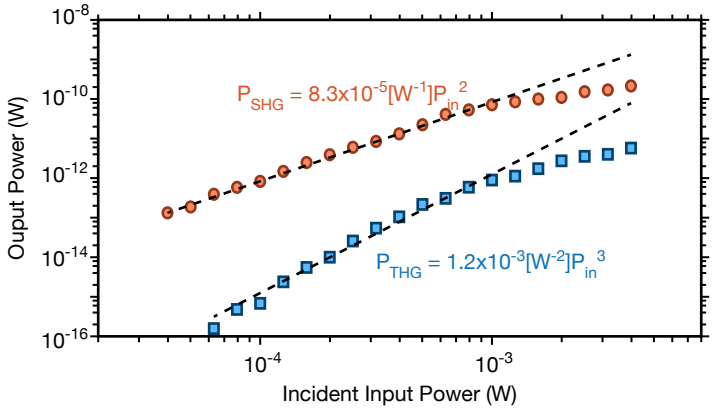

FIG. 4. Second (red circles) and third harmonic generation (blue squares) output power regarding input coupled power at 1.5 µm. The dashed lines correspond of a quadratic and cubic fit for SH and TH signal respectively and from which conversion efficiency is extracted.

order as the record of SHG observed in other III-V materials PhC cavities[20] and order of magnitude higher than previous work on GaAs[9] or Silicon[22] PhC cavities (*i.e.* non-resonant at SH wavelength). However, output powers could be increased thanks to SH resonance, design achievable using, for instance, micro-disk, where SH signal up to 0.5 nW was shown[21]. In our case, meaning non doubly-resonant SH or TH design, these values are achievable thanks to the high power density in the cavity, thanks to both high Q factor and small modal volume. Nevertheless, photo-induced oxidation was observed in our different uncoated sample and in the literature, mostly due to free carrier generation/recombination[23,24], blue shifting irreversibly the resonance. Thanks to the conformal encapsulation of the material through the ALD technique, no change in the resonance wavelength was observed, thus no photo-oxidation process.

Stability over input power is a key aspect of efficient SHG and THG. Indeed, GaAs undergoes photo-induced oxidation changing the refractive index of the resonator, thus the resonance frequency. Several different process can occur oxidizing the material such as thermally induced[10,23], catalytic effect of electron-hole pairs[25], hot carrier for efficient O_2 adsorption[26,27]. All those effects are directly linked with O_2 adsorption on the GaAs surface. In regards with the Telecom wavelength here, which generates carriers through Two-Photon Absorption (TPA) just above the band-gap, the main oxidation effect is the thermally induced one through carrier recombination[28], and enhanced by the high carrier surface recombination velocity[11,29]. Therefore, other processes can be considered as negligible.

To investigate further the oxidation process, we measure the temperature of the resonator, using two main different techniques. First by observing the modification of the photo-luminescence spectra (Fig. 5d) using an OSA (Thorlabs), the band gap energy can be probed (which correspond to the energy of the peak of photo-luminescence minus $k_BT/2$) and is directly linked to the temperature of the material as described in ref. 30. Secondly the spectral shift of the resonance measured by probing the THG (Fig. 5c), SHG (Fig. 5b) and the direct transmission at 1.5µm (Fig. 5a). Indeed, the GaAs ~~the~~ temperature rise induces a refractive index shift, following 31:

$$n = -1.86 \times 10^{-10}\frac{T^3}{3} + 3.49 \times 10^{-7}\frac{T^2}{2} + 1.47 \times 10^{-4}T + 3.431869 \quad (1)$$

Using FDTD computation, one can retrieve the dependence of the resonance wavelength with the refractive index of this specific device, such that:

$$\lambda = 5.1 \times 10^{-8}n^2 + 5.7 \times 10^{-8}n + 6.881 \times 10^{-7} \quad (2)$$

Fig 5e exhibits the coherence of the results through the four measurements, and mostly the consistency of the results through the two main types of characterization. A small wavelength detuning is measured in the transmission map between direct transmission compared to SH and TH ones, which was already observed in other nitride based material[32]. The maximum increase of the sample temperature is of about 135 K, and as the experiment are made at room temperature, to a resonator temperature of about 435 K during several minutes. Even after few experiments reaching this temperature, no modifications are observed in the resonance wavelength when the cavity has cooled down to room temperature.

In comparison, previous works shown that for an uncoated GaAs sample and heating it at a temperature of 435 K during 3 min, the PhC resonator exhibited a resonance spectral blue shift of 1.4 nm at room temperature. Thermally activated oxide thickness, therefore the wavelength shift[10], can be described by $\Delta\lambda_{res} \propto \sqrt{D_O}\exp\left(\frac{E_a}{2k_BT}\right)\sqrt{t}$, where D_O is the diffusivity of Oxygen in the material and E_a the activation energy. Our total experimental time is order of magnitude longer than the one shown in ref. 10 (experiments shown here are on the time scale of several minutes for the same input power, and have been repeated several time), without exhibiting any change in the resonance wavelength. We can then conclude that the ALD layer creates a barrier from the atmosphere, reducing drastically the diffusivity of oxygen into the GaAs, and then disabling photo-induced oxidation. It allows to reach high input power, thus high SH and TH output power.

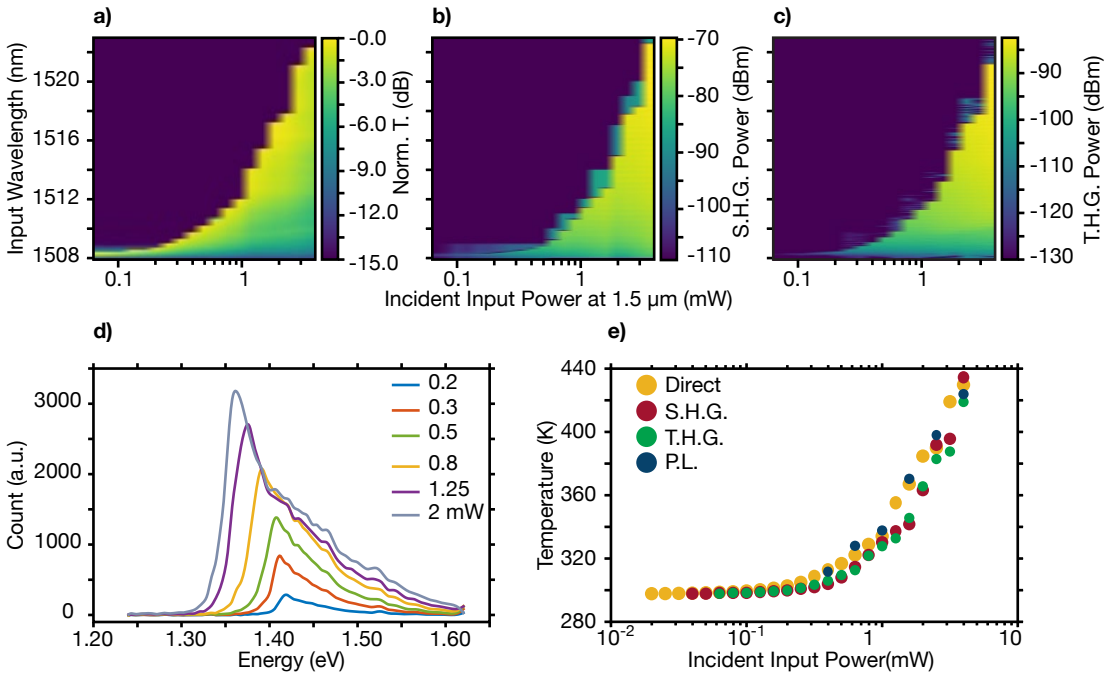

FIG. 5. Measurement of the transmission (colormap) of a) direct transmission at 1.5 µm b) SHG signal and c) THG signal versus the input power and the input wavelength. d) Measurement of the photoluminescence ~~of~~ for different input ~~power~~ at 1.5 µm. e) Extracted temperature of the cavity using the two methods, namely spectral shift (blue, red and green circles) and band-gap energy measurement (yellow cirles)

In conclusion, we have shown here high output power for SHG and THG in PhC resonator made of GaAs. Indeed, conform encapsulation of the material with Al_2O_3 made by ALD enables to prevent photo-induced oxidation leading to an irreversible blue shift of the resonance. Therefore, high input power can be injected into the system, leading to high output power. Measurement of the system temperature was achieved by measuring the shift of the resonance wavelength and by measuring the photo-luminescence spectra. The system reaches a maximum temperature of 435 K, without any degradation of the resonator. By improving the conversion efficiency of SH and TH operations, such system can be of great promise for high output power SHG, for instance for $f-2f$ optical clock systems, and high output THG for efficient sub-wavelength imaging.

This work was funded by Agence Nationale de la Recherche/DoD through contract ETHAN (ANR-15-ASTR-0014) and AUCTOPUSS (ANR-12-ASTR-0014).

REFERENCES

[1]Z. Zhang and M. Qiu, Opt. Exp. **12**, 3988 (2004).

[2]S. Combrié, A. de Rossi, Q. V. Tran, and H. Benisty, Opt. Lett. **33**, 1908 (2008).

[3]S. Combrié, Q. V. Tran, A. de Rossi, C. Husko, and P. Colman, Appl. Phys. Lett. **95**, 221108 (2009).

[4]Z. Han, X. Checoury, L.-D. Haret, and P. Boucaud, Opt. Lett. **36**, 1749 (2011).

[5]S. B. Papp, K. Beha, P. Del'Haye, F. Quinlan, H. Lee, K. J. Vahala, and S. A. Diddams, Optica **1**, 10 (2014).

[6]T. Udem, R. Holzwarth, and T. W. Hansch, Nature **416**, 233 (2002).

[7]Y. Barad, M. Horowitz, and Y. Silberberg (SPIE, 1997).

[8]Y. Zeng, I. Roland, X. Checoury, Z. Han, M. El Kurdi, S. Sauvage, B. Gayral, C. Brimont, T. Guillet, F. Semond, and P. Boucaud, ~~ACS Photonics (2016), 10.1021/acsphotonics.6b00236.~~

[9]S. Buckley, M. Radulaski, J. Petykiewicz, K. G. Lagoudakis, J.-H. Kang, M. Brongersma, K. Biermann, and J. Vučković, ACS Photonics **1**, 516 (2014).

[10]H. S. Lee, S. Kiravittaya, S. Kumar, J. D. Plumhof, L. Balet, L. H. Li, M. Francardi, A. Gerardino, A. Fiore, A. Rastelli, and O. G. Schmidt, Appl. Phys. Lett. **95**, 191109 (2009).

[11]G. Moille, S. Combrié, L. Morgenroth, G. Lehoucq, F. Neuilly, B. Hu, D. Decoster, and A. de Rossi, Laser Photon. Rev **10**, 409 (2016).

[12]Y. Akahane, T. Asano, B.-S. Song, and S. Noda, Nature **425**, 944 (2003).

[13]N.-V.-Q. Tran, S. Combrié, and A. de Rossi, Phys. Rev. B **79**, 041101 (2009).

[14]Q. V. Tran, S. Combrié, P. Colman, and A. de Rossi, Appl. Phys. Lett. **95**, 061105 (2009).

[15]R. W. Boyd, *Nonlinear Optics* (Academic Press, 2013).

[16]J. Sipe, D. Moss, and H. van Driel, Phys. Rev. B **35**, 1129 (1987).

[17]D. E. Aspnes, S. M. Kelso, R. A. Logan, and R. Bhat, Journal of Applied Physics **60**, 754 (1986).

[18]G. Jellison, Optical Materials **1**, 151 (1992).

[19]C. Manolatou, M. J. Khan, S. Fan, P. R. Villeneuve, H. A. Haus, and J. D. Joannopoulos, IEEE J. Quantum Electron. **35**, 1322 (1999).

[20]K. Rivoire, Z. Lin, F. Hatami, W. T. Masselink, and J. Vučković, Opt. Exp. **17**, 22609

(2009).

[21]P. S. Kuo, J. Bravo-Abad, and G. S. Solomon, Nat Comms **5**, 1 (2014).

[22]M. Galli, D. Gerace, K. Welna, T. F. Krauss, L. O'Faolain, G. Guizzetti, and L. C. Andreani, Opt. Exp. **18**, 26613 (2010).

[23]M. Fukuda and K. Takahei, J. Appl. Phys **57**, 129 (1985).

[24]S. A. Schafer and S. A. Lyon, J. Vac. Sci. Technol. **19**, 494 (1981).

[25]F. Intonti, N. Caselli, S. Vignolini, F. Riboli, S. Kumar, A. Rastelli, O. G. Schmidt, M. Francardi, A. Gerardino, L. Balet, L. H. Li, A. Fiore, and M. Gurioli, Appl. Phys. Lett. **100**, 033116 (2012).

[26]C. F. Yu, M. T. Schmidt, D. V. Podlesnik, and R. M. Osgood Jr, J. Vac. Sci. Technol. B **5**, 1087 (1987).

[27]Z. Lu, M. T. Schmidt, D. V. Podlesnik, C. F. Yu, and R. M. Osgood, J. Chem. Phys. **93**, 7951 (1990).

[28]W. G. Petro, I. Hino, S. Eglash, I. Lindau, C. Y. Su, and W. E. Spicer, J. Vac. Sci. Technol. **21**, 405 (1982).

[29]D. D. Nolte, Solid-State Electron. **33**, 295 (1990).

[30]S. Gehrsitz, F. K. Reinhart, C. Gourgon, N. Herres, A. Vonlanthen, and H. Sigg, J. Appl. Phys **87**, 7825 (2000).

[31]F. G. Della Corte, G. Cocorullo, M. Iodice, and I. Rendina, Appl. Phys. Lett. **77**, 1614 (2000).

[32]Y. Zeng, I. Roland, X. Checoury, Z. Han, M. El Kurdi, S. Sauvage, B. Gayral, C. Brimont, T. Guillet, M. Mexis, F. Semond, and P. Boucaud, Appl. Phys. Lett. **106**, 081105 (2015).